Detection of a radial velocity gradient in the extended local disc with RAVE

A. Siebert,[1]⋆ B. Famaey,[1] I. Minchev,[1] G. M. Seabroke,[2] J. Binney,[3] B. Burnett,[3]
K. C. Freeman,[4] M. Williams,[5] O. Bienaymé,[1] J. Bland-Hawthorn,[6] R. Campbell,[5]
J. P. Fulbright,[7] B. K. Gibson,[8] G. Gilmore,[9] E. K. Grebel,[10] A. Helmi,[11] U. Munari,[12]
J. F. Navarro,[13] Q. A. Parker,[14] W. A. Reid,[14] A. Siviero,[5,12] M. Steinmetz,[5]
F. Watson,[15] R. F. G. Wyse[7] and T. Zwitter[16,17]

[1]*Observatoire Astronomique, Université de Strasbourg, CNRS, 11 rue de l'université, 6700 Strasbourg, France*
[2]*Mullard Space Science Laboratory, University College London, Holmbury St Mary, Dorking RH5 6NT*
[3]*Rudolf Peierls Centre for Theoretical Physics, 1 Keble Road, Oxford OX1 3NP*
[4]*Research School of Astronomy and Astrophysics, Australian National University, Cotter Road, Weston Creek, ACT 2611, Australia*
[5]*Astrophysikalishes Institut Potsdam, An der Sternwarte 16, D-14482 Potsdam, Germany*
[6]*Sydney Institute for Astronomy, School of Physics A29, University of Sydney, NSW 2006, Australia*
[7]*Johns Hopkins University, Department of Physics and Astronomy, 366 Bloomberg Center, 3400 N.Charles Street, Baltimore, MD 21218, USA*
[8]*Jeremiah Horrocks Institute, University of Central Lancashire, Preston PR1 2HE*
[9]*Institute of Astronomy, University of Cambridge, Madingley Road, Cambridge CB3 OHA*
[10]*Astronomisches Rechen-Institut, Zentrum für Astronomie der Universität Heidelberg, Nönchhofstrasse 12.14, D-69120 Heidelberg, Germany*
[11]*Kapteyn Astronomical Institut, University of Groningen, Landleven 12, 9747 AD Groningen, the Netherlands*
[12]*INAF Astronomical Observatory of Padova, 36012 Asiago (VI), Italy*
[13]*Department of Physics and Astronomy, University of Victoria, P.O. Box 3055, Victoria, BC V8W 3P6, Canada*
[14]*Department of Physics and Astronomy, Faculty of Science, Macquarrie University, NSW 2109, Sydney, Australia*
[15]*Australian Astronomical Observatory, P.O. Box 296, Epping, NSW 1710, Australia*
[16]*Faculty of Mathematics and Physics, University of Ljubljana, Jadranska 19, 1000 Ljubljana, Slovenia*
[17]*Center of excellence, SPACE-SI, Aškerčeva cesta 12, 1000 Ljubljana, Slovenia*

ABSTRACT

Using a sample of 213 713 stars from the Radial Velocity Experiment (RAVE) survey, limited to a distance of 2 kpc from the Sun and to $|z| < 1$ kpc, we report the detection of a velocity gradient of disc stars in the fourth quadrant, directed radially from the Galactic Centre. In the direction of the Galactic Centre, we apply a simple method independent of stellar proper motions and of Galactic parameters to assess the existence of this gradient in the RAVE data. This velocity gradient corresponds to $|K + C| \gtrsim 3$ km s^{-1} kpc^{-1}, where K and C are the Oort constants measuring the local divergence and radial shear of the velocity field, respectively. In order to illustrate the effect, assuming a zero radial velocity of the local standard of rest we then reconstruct the two-dimensional Galactocentric velocity maps using two different sets of proper motions and photometric distances based either on isochrone fitting or on K-band magnitudes, and considering two sets of values for the Galactocentric radius of the Sun and local circular speed. Further observational confirmation of our finding with line-of-sight velocities of stars at low latitudes, together with further modelling, should help constrain the non-axisymmetric components of the Galactic potential, including the bar, the spiral arms and possibly the ellipticity of the dark halo.

Key words: stars: kinematics and dynamics – Galaxy: fundamental parameters – Galaxy: kinematics and dynamics.

1 INTRODUCTION

Our Milky Way Galaxy is a unique laboratory in which to study galactic structure and evolution from stellar kinematics. The story

⋆E-mail: arnaud.siebert@astro.unistra.fr

of the efforts to obtain such kinematic data nicely illustrates how theoretical progress and data acquisition have to go hand in hand if one wants to gain insight into the structure and history of the Galaxy. Until recently, most studies have been limited to the solar neighbourhood. The zeroth-order approximation for modelling these kinematic data assumes an axisymmetric model, in which the local standard of rest (LSR) is on a perfectly circular orbit. However, the local velocity field in the solar neighbourhood already displays possible signatures of the non-axisymmetry of the Galactic potential in the form of stellar moving groups containing stars of very different ages and chemical compositions (Dehnen 1998; Famaey et al. 2005; Quillen & Minchev 2005; Bensby et al. 2007; Minchev et al. 2010).

In external galaxies, large-scale distortions of the (line-of-sight) isovelocity contours of the gas have long been recognized in two-dimensional velocity maps (e.g. Bosma 1978), allowing a quantification of the strength of non-circular streaming motions (e.g. Sellwood & Zanmar Sanchez 2010). A prominent example is the galaxy M81 (e.g. Adler & Wefstpfahl 1996), which has roughly the same circular velocity as the Milky Way and in which the radial streaming motions of the gas reach maxima of the order of $50 \, \mathrm{km \, s^{-1}}$. However, the stellar kinematics often turn out to be slightly more regular and symmetric than the gas kinematics (e.g. Pizzella et al. 2008). For instance, Rix & Zaritsky (1995) estimate from 18 face-on spiral galaxies that the azimuthally averaged radial streaming motions of disc stars should typically amount to a maximum of $7 \, \mathrm{km \, s^{-1}}$ due to lopsided distortions and $6 \, \mathrm{km \, s^{-1}}$ due to intrinsic ellipticity.

In the Milky Way, non-axisymmetric motions are clearly visible in radio-frequency observations of gas flow in the inner Galaxy, implying that the amplitude of spiral structure could be larger by a factor of ~ 1.5 than its amplitude in the near-infrared luminosity density (Bissantz et al. 2003; Famaey & Binney 2005). On the other hand, radio interferometry used to determine the parallax of star-forming regions in the Perseus spiral arm, together with the measurement of their line-of-sight (los) velocities, show that these star-forming regions have peculiar non-circular motions amounting to $\sim 20 \, \mathrm{km \, s^{-1}}$, assuming standard IAU Galactic parameters and a nearly flat rotation curve (Binney 2006; Xu et al. 2006; Reid et al. 2009). However, the amplitude of such non-circular motions strongly depends on the Galactic parameters adopted (McMillan & Binney 2010), namely the Galactocentric radius of the Sun R_0, the local circular speed v_{c0} and the reflex solar motion, as well as on the model for the rotation curve. Another example of such non-circular motion is the 3-kpc arm which has $v_{los} = -80 \, \mathrm{km \, s^{-1}}$ towards the Galactic centre (GC) and is known to have a counterpart on the far side of the GC (Dame & Thaddeus 2008). Its origin is associated to the Galactic bar showing that non-circular motion of similar amplitude can be caused by various types of perturbations and not necessarily by spiral arms.

Here, we use line-of-sight velocity[1] data (v_{los}) from the RAVE survey to investigate whether the mean radial motion of disc stars remains zero in the extended solar neighbourhood as compared to the one in the solar neighbourhood, or whether large-scale radial streaming motions are present in the vicinity of the Sun, which would translate in a radial velocity gradient in one or the other direction. In Section 2 we present the sample used for our analysis

while in Section 3 we present the detection of a radial velocity gradient using RAVE v_{los}, as well as the associated Oort constants and two-dimensional velocity field. Finally in Section 4 we discuss the implications of our results and present our conclusions.

2 THE RAVE SAMPLE

Our analysis is based on the RAVE catalogue (Steinmetz et al. 2006; Zwitter et al. 2008) which provides v_{los} to $2 \, \mathrm{km \, s^{-1}}$ and stellar atmospheric parameters and distances to 30 per cent for a large number of bright stars in the Southern hemisphere with $9 < I < 12$ using moderate resolution spectra ($R \sim 7500$). RAVE selects its targets randomly in the I-band interval, and so its properties are similar to a magnitude limited survey. The RAVE catalogue is cross-matched with astrometric (PPMX, UCAC2, Tycho-2) and photometric catalogues (2MASS, DENIS) to provide additional proper motions and magnitudes making RAVE a suitable tool to study the Milky Way.

We use the latest version of the Zwitter et al. (2010) catalogue, which contains four sets of distances in addition to the standard RAVE data (line-of-sight velocities and stellar parameters). These four sets of distances are (i) the distance moduli computed using three sets of isochrones (including the Padova isochrones), and (ii) the distances of Breddels et al. (2010). In this paper we will use the distance moduli based on the Padova isochrones but our results do not strongly depend on the set of isochrones used (see also Section 3.2 where all distances are multiplied by an arbitrary factor). This catalogue is cleaned from potentially problematic fields using a list kindly provided by G. Matijevic (private communication) and we further select stars with $|z| < 1 \, \mathrm{kpc}$ to minimize contamination by halo stars. This leaves us with a sample of 213 713 stars with known distances, atmospheric parameters ($\log g$, T_{eff}, $[m/H]$), proper motions as well as v_{los} measurements that can be used to compute the 3D space velocities.

To verify that our analysis does not depend on the method used to determine the distances or on the source of proper motions, we also use stars for which distances and proper motions are obtained independently. To do so, we select a subsample of red clump candidates for which the distance can be estimated using the K magnitude alone because of the narrow, almost Gaussian, luminosity function of the red clump. Red clump candidates are selected in the ($\log g$, $J - K$) plane, as illustrated in Fig. 1. We select the overdensity using $0.5 < J - K < 0.735$ and $1.8 < \log g < 2.8$: the red limit helps reduce the contamination by the upper red giant branch stars. Distances are obtained assuming all stars in the sample are red clump stars using a Gaussian luminosity function for this population with $M_K = -1.6$ and $\sigma_K = 0.22$. We apply the same cut in z as for the full sample. This results in a sample containing 29 623 red clump candidates. More details on the contamination and distance errors can be found in Siebert et al. (2008). We cross-match this sample with the UCAC3 catalogue to provide a different source for the proper motion – the RAVE catalogue contains predominantly Tycho-2 and PPMX proper motions. Hence, for this sample, the distances and proper motions are independent from the full RAVE sample. The mean height above/below the Galactic plane for each sample is shown in Fig. 2.

3 A RADIAL VELOCITY GRADIENT

3.1 Line-of-sight velocity detection

Most of the RAVE stars lie in the fourth Galactic quadrant with the tails of the distribution in Galactic longitude extending in the
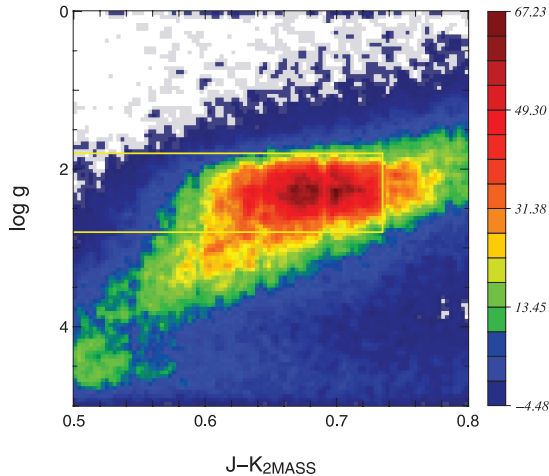

Figure 1. Distribution of stars in the $(\log g, J - K)$ plane near the red clump for the RAVE internal release. Colour coding follows the number of stars per bin of 0.03 mag width in $J - K$ and 0.05 dex in $\log g$. The distribution is smoothed over 3 pixels to reduce the noise. Stars in the white box are identified as red clump stars.

first and third quadrants. For our analysis to remain independent of Galactic parameters and proper motions, we first look in the GC (and anticentre) direction with $|l| < 5°$ (and $175° < l < 185°$). In this case, the Galactocentric radial velocity is close to the measured line-of-sight velocity projected on the plane (or its opposite in the anticentre direction), with only a small contribution from the proper motion vector.

In Fig. 3 we plot the projection on to the plane of the mean v_{los} in bins 200 pc wide as a function of $d \cos b$. The left-hand panel is for the full sample and the right-hand panel for the red clump candidates. We then compare the observed mean velocities to the expected velocities for a thin disc in circular rotation at v_{c0} and adding a radial gradient $\partial \langle V_R \rangle / \partial R = 3, 5$ and $10 \, \mathrm{km \, s^{-1} \, kpc^{-1}}$, where V_R is the Galactocentric radial velocity (see full curves from top to bottom in each panel in Fig. 3). The curves are drawn using 5000 Monte Carlo realizations of the samples, replacing the measured velocities by random realizations of a thin disc ellipsoid. The model used is the same for both samples, kinematic parameters for the thin disc ellipsoid being taken from Binney & Merrifield (1998)
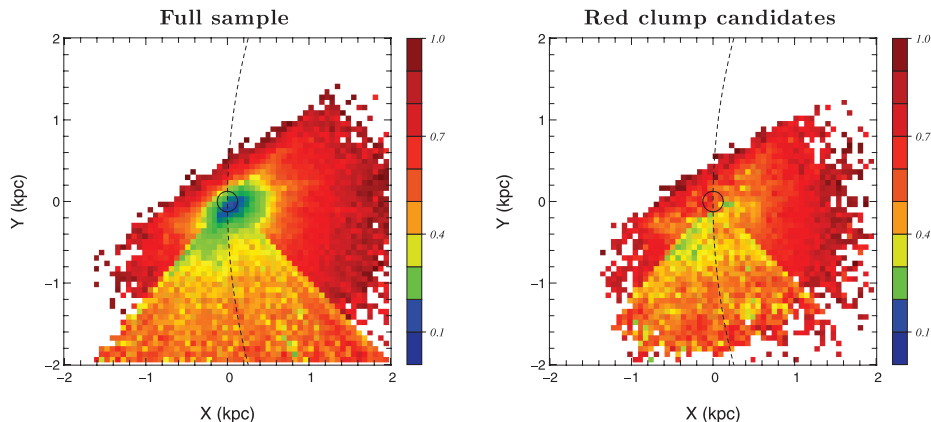
table 10.4. Clearly, our data are not compatible with a disc in circular rotation because the mean projected line-of-sight velocity is systematically lower than the expected mean velocity. The offset between the two panels reflects the different distribution in R of the two samples.

Because our samples are not perfectly oriented towards the GC, the rotation component could bias our measurement. Therefore, we reproduce this by modelling a thick disc population which lags the circular rotation by $36 \, \mathrm{km \, s^{-1}}$. The result for a thick disc is presented as dashed curves and is computed only in the case of circular rotation. The results do not differ significantly from the thin disc results indicating that the contribution from v_{c0} to our line-of-sight velocities is marginal and hence that our result truly measures a radial velocity gradient in the RAVE data.

3.2 Oort constants

As first worked out by Oort (1927) for an axisymmetric Galaxy, and later generalized to non-axisymmetry (e.g. Chandrasekhar 1942), a practical way to study the global streaming motion of field stars in the Galaxy is to consider an arbitrary smooth velocity field and Taylor expand it around the position of the Sun. Such a Taylor expansion of the Cartesian velocity components (U, V) to first order yields the four Oort constants A, B, C and K, measuring the azimuthal (A) and radial (C) shear, the local divergence (K) and the vorticity (B) of the velocity field (see e.g. Kuijken & Tremaine 1994; Olling & Dehnen 2003, hereafter KT94 and OD03, respectively).

While we note that such a first-order Taylor expansion might not be a valid description of the velocity field for sample depths larger than 1 kpc (as already noted in Pont, Mayor & Burki 1994; OD03), we also note that, at least in the direction of the GC, a constant linear velocity gradient $\partial V_R / \partial R = K + C$ between -3 and $-10 \, \mathrm{km \, s^{-1} \, kpc^{-1}}$ is sufficient to reproduce the trend seen in Fig. 3. In view of this, we compute the Oort constants in the classical way using

$$\langle v_{rad}/r \rangle = K + A \sin 2\ell + C \cos 2\ell,$$
$$\langle v_t/r \rangle = B + A \cos 2\ell - C \sin 2\ell, \qquad (1)$$

where v_{rad} (resp. v_t) is the heliocentric radial (resp. transverse) component of the velocity vector in the Galactic plane corrected for the motion of the Sun with respect to the LSR. r is the distance from the star to the Sun in the Galactic plane and A, B, C and K are

Figure 2. Mean $|z|$ distance to the Galactic plane in kpc for the two samples studied: full sample (left), red clump sample (right). The two panels contain 60×60 pixels in a box 4×4 kpc in extent. Both samples have an upper limit on $|z|$, $\max(|z|) = 1$ kpc. The Sun is located at the centre of the map, X is increasing in the direction of the GC and Y towards the Galactic rotation. The solar circle is shown as a dashed line. The circle in the centre represents a sphere 125 pc in radius.
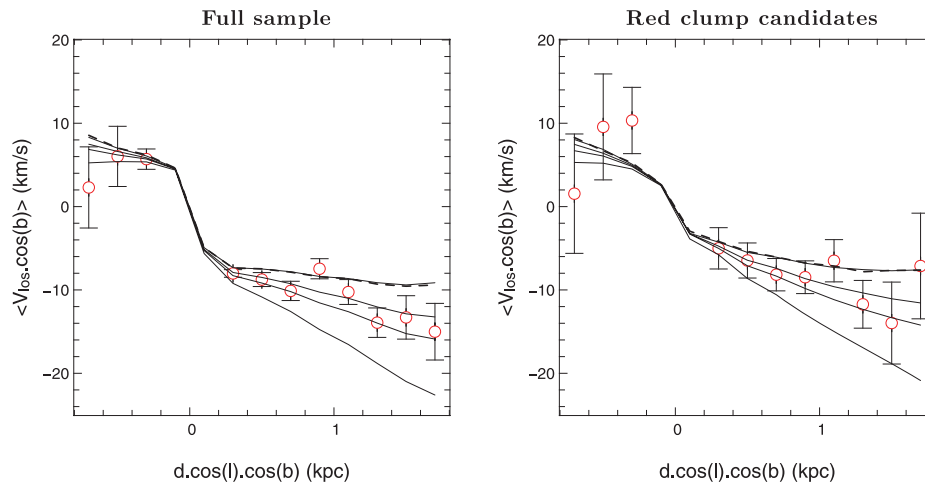
Figure 3. Projection of the mean RAVE v_{los} on the Galactic plane in distance intervals of 200 pc in the direction of the GC ($|l| < 5°$) and anticentre ($175° < l < 185°$) for our two samples. Left: full sample containing 10 682 stars. Right: red clump sample containing 1328 stars. The open circles are our data with 1σ error bars. The dashed curve corresponds to a thick disc model with no net radial motion, while the full curves are for a thin disc with a radial velocity gradient of 0, 3, 5 and 10 km s^{-1} kpc^{-1} from top to bottom.

Table 1. Oort constants A, B, C and K measured using the RAVE sample. The kinematic centre $\psi_v = 0.5 \arctan(-C/A)$, the amplitude $\sqrt{A^2 + C^2}$ and the velocity gradient $\partial V_R / \partial R = K + C$ are also given. All numbers (apart from ψ_v) are in km s^{-1} kpc^{-1}. The first two lines give the old values from KT94 and OD03. For the RAVE sample, errors bars are computed using a Monte Carlo sampling, but they do not take into account the possible systematics listed in OD03. The last two lines show changes in the Oort constants if one considers a 20 per cent bias in our distances. The two cases are obtained by multiplying the distances of the whole catalogue by 0.8 or 1.2, then recomputing the velocities and re-applying the same R, z selection as before.

	Sample	A	B	C	K	ψ_v (°)	$\sqrt{A^2 + C^2}$	$K + C$
KT94	v_{los}, μ_b and μ_l	14.4 ± 1	-12.0 ± 3	0.6 ± 1	-0.35 ± 0.5	-1.2	14.4	0.25
OD03	μ_l	15.9 ± 2	-16.9 ± 2	-9.8 ± 2	–	15.5	18.7	–
RAVE	v_{los} and μ_b	13.6 ± 0.5	–	-9.6 ± 0.5	5.7 ± 0.3	17.6	16.6	-3.9
RAVE	v_{los}, μ_b and μ_l	9.2 ± 0.5	-17.4 ± 0.5	-12.7 ± 0.5	4.6 ± 0.5	27.0	15.7	-8.1
$d \times 0.8$	v_{los} and μ_b	15.0	–	-9.2	6.3	15.8	17.6	-2.9
$d \times 0.8$	v_{los}, μ_b and μ_l	11.1	-11.8	-10.5	5.6	21.7	15.3	-4.9
$d \times 1.2$	v_{los} and μ_b	12.5	–	-10.1	5.3	19.5	16.1	-4.8
$d \times 1.2$	v_{los}, μ_b and μ_l	7.9	-21.3	-14.4	4.1	30.6	16.4	-10.3

the Oort constants we try to measure (see also KT94; OD03). We then fit the right-hand side of equation (1) to the left-hand side that is built upon our observations with v_{rad} depending on v_{los} and μ_b while v_t depends on μ_ℓ.

We restrict the sample to the $-140° < \ell < 10°$ interval, the noise in the computed mean velocities preventing a reliable fit outside of this interval. In order not to rely too much on the proper motions and mostly on RAVE data, the median proper motion error of the sample being 1.8 mas yr^{-1}, we first fit only the constants A, C and K to the line-of-sight velocity *in the Galactic plane* v_{rad}, thus using only v_{los} and μ_b. We then use all the available information, and thus fit also the constants A, B and C to the tangential velocity in the plane (based on μ_l). Once the Oort constants are fitted to the mean velocity field of the observed population, we correct them for the asymmetric drift as in OD03: since the RAVE catalogue is dominated by the old thin disc, we use an asymmetric drift of 20 km s^{-1}. The results are listed in Table 1, and compared to those of KT94 and OD03. We note that, although we used the updated values of Schönrich, Binney & Dehnen (2010) for the reflex motion of the Sun, our value for C, especially when fitting only the line-of-sight velocity in the Galactic plane, is in remarkable agreement with the value found by OD03 (after the mode-mixing correction) from proper motions

of old red giants[2] in the ACT/Tycho-2 catalogues. However, our value of C (and K) is in disagreement with the one reported in KT94 from a review of the older literature. Let us finally note that the formal errors quoted in Table 1 were computed using a Monte Carlo sampling but are large underestimations of the true errors, due to possible systematics including those listed in OD03, as well as the absence of a full longitude coverage. This underestimation of the errors is confirmed by the fact that, when taking or not taking into account the longitudinal proper motions, the values of the Oort constants A and C differ by more than 6 formal sigmas and 4 formal sigmas, respectively. The fit to v_{rad} alone (third line of Table 1) is more reliable as it mostly relies on the RAVE line-of-sight velocities and is of better quality than the one including longitudinal proper motions (the reduced χ^2 values are 1.4 and 2.6, respectively).

This fitting procedure of the Oort constants thus confirmed our finding of Section 3.1 that $|\partial V_R / \partial R| \gtrsim 3$ km s^{-1} kpc^{-1} in the RAVE

---

[2] OD03 found different values for different populations (especially, lower $|C|$ for lower velocity dispersion populations), but their best tracers of the 'true' Oort constants are the red giants, also affected by an asymmetric drift of roughly 20 km s^{-1}.
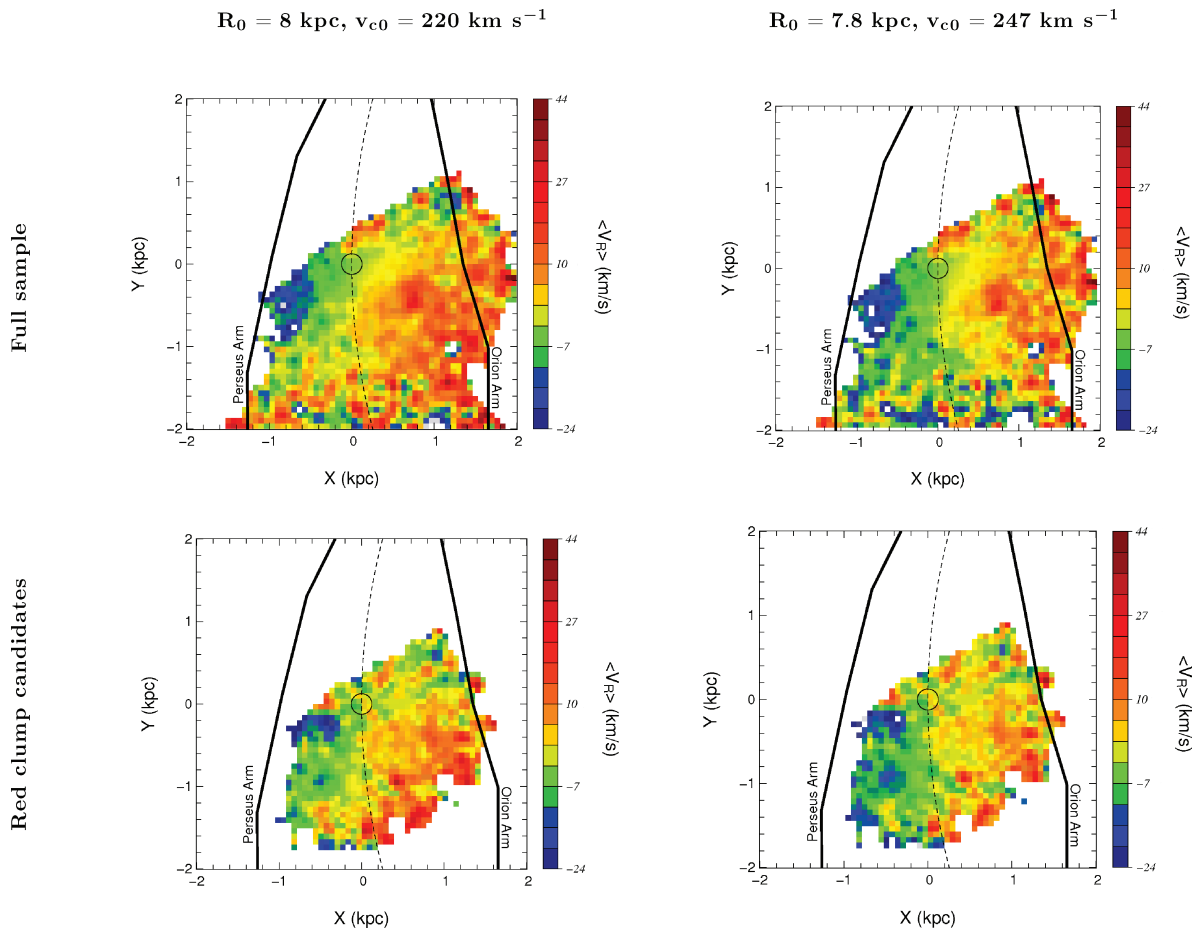
Figure 4. Mean velocity fields $\langle V_R \rangle$ derived using equation (2) and assuming $R_0 = 8$ kpc and $v_{c0} = 220$ km s^{-1} (left-hand panels) and $R_0 = 7.8$ kpc and $v_{c0} = 247$ km s^{-1} (right-hand panels). Top panels: full sample. Bottom panels: red clump selection. The locations of the nearest spiral arms are indicated using the CO map from Englmaier et al. (2008). The open circle delimitates a sphere 125 pc in radius around the Sun. The maps are smoothed over 3 pixels to highlight the mean velocity trends. The maps are 60×60 bins in size between -2 and 2 kpc along each axis. X increases in the direction of the GC and Y is positive towards the Galactic rotation.

catalogue. Let us note that, as we rely on a priori known distances, our result is not affected by mode mixing. However, in order to check whether the qualitative conclusion of the existence of non-zero velocity gradient depends on our estimates of the distances, we assumed that all distances were wrong by a factor f, and re-applied the same procedure. Results for $f = 0.8$ and 1.2 are listed at the end of Table 1, confirming that $K + C \neq 0$ in both cases.

3.3 Two-dimensional velocity field

To further investigate the velocity gradient detected with RAVE, we now compute the full 2D velocity field for our samples (making use of both the line-of-sight velocities and the proper motion vectors).

The velocity fields in the Galactocentric reference frame are computed using

$$V_{GSR} = V_{*/\odot} + V_{\odot/LSR} + V_{LSR/GSR}, \qquad (2)$$

where $V_{\odot/LSR}$ is the Sun's velocity with respect to the LSR and $V_{LSR/GSR}$ is the motion of the LSR with respect to the GC. Obviously, a possible radial motion of the LSR itself can be a priori difficult to disentangle from large-scale streaming motions. In order to circumvent this, we use hereafter the standard assumption

that the LSR is on a circular orbit.[3] The velocity of stars V_{GSR} is hereafter decomposed into three components in the axisymmetric galactocentric reference frame (V_R, V_ϕ, V_z), V_z pointing towards the South Galactic Pole.

This projection depends on two parameters: R_0, the distance to the centre of the Galaxy, and v_{c0}, the local circular speed. Unfortunately, as pointed out by McMillan & Binney (2010), neither of these parameters are well constrained. The ratio v_{c0}/R_0 is however better constrained, lying in the range 29.9–31.6 km s^{-1} kpc^{-1} with some impact on the measured $V_{\odot/LSR}$ as shown in tables 1 and 2 of McMillan & Binney (2010).

Therefore, we compute the 2D velocity maps for two sets of parameters. In both cases we fix $V_{\odot/LSR}$ to the values of Schönrich et al. (2010). The first set of parameters uses the standard IAU values $v_{c0} = 220$ km s^{-1} and $R_0 = 8$ kpc, while for the second set we use the model 2 from table 2 of McMillan & Binney (2010), $v_{c0} = 247$ km s^{-1} and $R_0 = 7.8$ kpc, which has a solar motion vector close to the latest determination by Schönrich et al. (2010).

The results for the 2D $\langle V_R \rangle$ and $\langle V_\phi \rangle$ velocity maps in the Galactic plane for a 4×4 kpc box (60×60 bins) centred on the Sun are presented in Figs 4 and 5 for both sets of parameters and for both

---

[3] Although this does not formally exist in a non-axisymmetric potential.
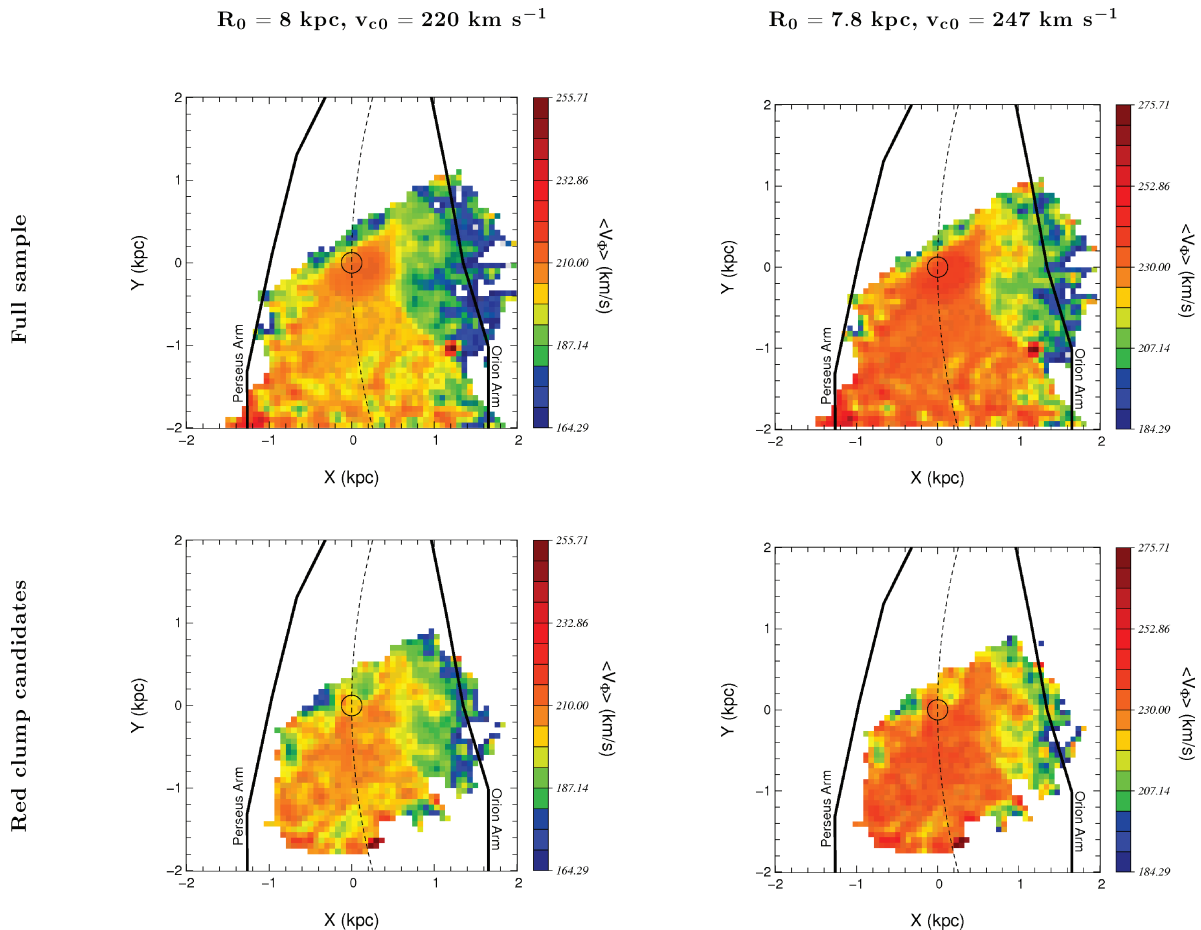
Figure 5. Same as Fig. 4 but for $\langle V_\phi \rangle$.

samples (full sample and red clump selection). X and Y increase towards the GC and in the direction of Galactic rotation, respectively. This places the GC either at (8, 0) or (7.8, 0) depending on the Galactic parameters used. The solar circle ($R = R_0$) is drawn as a dashed line and the open circle delimits a zone 125 pc in radius similar to the *Hipparcos* sphere. For orientation, the location of the local (Orion) and Perseus arms are indicated based on the CO map of Englmaier, Pohl & Bissantz (2008). No strong kinematic signal is associated with them in $\langle V_R \rangle$, but a strong decrease of $\langle V_\phi \rangle$ is associated with the Orion arm (while little data are available on the Perseus arm). This could help place limits on the size of the potential perturbations associated with these arms, but is beyond the scope of this paper.

Again, the global structure of the velocity field in Figs 4 and 5, comparing the top and bottom panels, is similar for both samples. Small differences exist on local scales, especially around $(X, Y) = (0.8, -0.4)$, but aside from this region the velocity trends are compatible. Isocontours in $\langle V_R \rangle$ are oriented about 50° from the direction to the GC and do not follow a particular symmetry axis of our procedure or sample. Within the local neighbourhood indicated by the open circle, no net motion is detected and our values are compatible with previous measurements. The velocity gradient becomes noticeable only outside the *Hipparcos* sphere.

Comparing left- and right-hand panels of Figs 4 and 5, we see that using updated Galactic parameters does influence the measured mean motions. In particular, in Fig. 4 it diminishes but does not eliminate the mean motions. Trying to minimize the gradient while

keeping the ratio v_{c0}/R_0 constant, leads to unrealistic values for the Galactic parameters with $R_0 < 4$ kpc and $v_{c0} < 126$ km s^{-1}.

4 DISCUSSION AND CONCLUSIONS

In this paper, making use of RAVE line-of-sight velocities and distances alone, we report the discovery of a radial velocity gradient in the Galactic disc amounting to at least 3 km s^{-1} kpc^{-1} observed in the direction of the GC for $d < 2$ kpc. Making use of the full sample, we fitted the Oort constants in the classical way, and obtained values globally in agreement with those of OD03 for old red giants. However as their measurement was based on proper motions alone, they could not constrain the value of the Oort constant K, which we estimate here to be roughly between 4 and 6 km s^{-1} kpc^{-1} (see Table 1).

Then, assuming a zero radial velocity of the LSR, we reconstructed the 2D velocity map, and found that the Galactic parameters do play a role in the measured amplitude of the streaming motion. Adopting standard IAU values, which are suspected to underestimate v_{c0}/R_0, yields a larger amplitude. On the other hand, using more recent values for v_{c0} and R_0 reduces the net radial motion but does not eliminate it. The latter result is independent of the source of proper motions and distances used. We note that the confirmed existence of such a net outwards motion for stars, amounting to 10 per cent of the circular speed, would raise the question of the validity of determining the Galactic parameters based on the assumption of circular motion (see e.g. Reid et al. 2009), and the

error bars on the measured ratio v_{c0}/R_0 are likely underestimated. We however also note that, in order to establish it more firmly, our result should imperatively be confirmed by further line-of-sight velocity measurements at lower latitudes with future spectroscopic surveys (see e.g. Minchev & Quillen 2008). It is indeed very intriguing that a strong 21-cm absorption feature along the line of sight to the GC is compatible with a zero mean velocity relative to the LSR (Radhakrishnan & Sarma 1980).

The cause of such a large-scale streaming motion would clearly be a non-axisymmetric component of the Galactic potential. It could thus be due to (i) the Galactic bar, (ii) spiral arms, (iii) the warp, (iv) a triaxial dark matter halo or (v) a combination of some or all of these components. Indeed, Minchev & Quillen (2007) have simulated the effect of spiral density waves on the Oort constants and have showed that for spiral-only perturbations, the value of $|C|$ is larger for lower stellar velocity dispersions, contrary to the findings of OD03. The observed trend in C could, however, be explained with the effect of the Galactic bar (Minchev, Nordhaus & Quillen 2007), but not its exact magnitude. Actually, given that the Milky Way disc contains both spiral arms and a central bar, the effect of both these perturbers needs to be considered simultaneously. In external galaxies, such as M81, such non-circular motions in gas flows are usually associated with spiral arms and/or the central bar. Sellwood & Zanmar Sanchez (2010) have also placed bounds on the ellipticity of the outer dark matter haloes of external galaxies from the observed non-circular motions (see also Binney 1978; Franx & de Zeeuw 1992; KT94). It will be of the highest interest to determine which model will best reproduce the trend we report in this paper. However, it is unlikely that we will be able to discriminate between the various models with such a small fraction of the Milky Way sampled. More, deeper observations from future astrometric and spectroscopic surveys will probably be mandatory in this respect.

Observations of non-circular motions of gas in the inner Galaxy determine the characteristics of the central region of the Milky Way and constrain the parameters of, for example, the Galactic bar and the amount of dark matter allowed inside the solar circle (see, for instance, Bissantz et al. 2003; Famaey & Binney 2005). It is likely that mapping and understanding the non-circular motions in the outer parts of the Milky Way will reveal similarly important information about the Galactic potential and the mass distribution on larger scales.

ACKNOWLEDGMENTS

REFERENCES

Adler D., Wefstpfahl D., 1996, AJ, 111, 735
Bensby T., Oey M. S., Feltzing S., Gustafsson B., 2007, ApJ, 655, L89
Binney J., 1978, MNRAS, 183, 779
Binney J., 2006, Sci, 311, 44
Binney J., Merrifield M., 1998, Galactic Astronomy. Princeton Univ. Press, Princeton, NJ
Bissantz N., Englmaier P., Gerhard O., 2003, MNRAS, 340, 949
Bosma A., 1978, PhD thesis, Univ. Groningen
Breddels M. A. et al., 2010, A&A, 511, 90
Chandrasekhar S., 1942, Principles of Stellar Dynamics. University of Chicago Press, Chicago, IL
Dame T. M., Thaddeus P., 2008, ApJ, 683, L143
Dehnen W., 1998, AJ, 115, 2384
Englmaier P., Pohl M., Bissantz N., 2008, in Corsini E. N., Debattista V. P., eds, Tumbling, Twisting, and winding Galaxies: Pattern Speeds along the Hubble Sequence. Memorie della Società Astronomica Italiana, Padova, Italy, p.199 (arXiv:0812.3491)
Famaey B., Binney J., 2005, MNRAS, 363, 603
Famaey B., Jorissen A., Luri X., Mayor M., Udry S., Dejonghe H., Turon C., 2005, A&A, 430, 165
Franx M., de Zeeuw T., 1992, ApJ, 392, L47
Kuijken K., Tremaine S., 1994, ApJ, 421, 178 (KT94)
McMillan P. J., Binney J., 2010, MNRAS, 402, 934
Minchev I., Quillen A. C., 2007, MNRAS, 377, 1163
Minchev I., Quillen A. C., 2008, MNRAS, 386, 1579
Minchev I., Nordhaus J., Quillen A. C., 2007, ApJ, 664, L31
Minchev I., Boily C., Siebert A., Bienaymé O., 2010, MNRAS, 407, 2122
Olling R., Dehnen W., 2003, ApJ, 599, 275 (OD03)
Oort J. H., 1927, Bull. Astron. Inst. Netherlands, 3, 275
Pizzella A., Corsini E. M., Sarzi M., Magorrian J., Méndez-Abreu J., Coccato L., Morelli L., Bertola F., 2008, MNRAS, 387, 1099
Pont F., Mayor M., Burki G., 1994, A&A, 285, 415
Quillen A. C., Minchev I., 2005, AJ, 130, 576
Radhakrishnan V., Sarma N. V. G., 1980, A&A, 85, 249
Reid M. J. et al., 2009, ApJ, 700, 137
Rix H.-W., Zaritsky D., 1995, ApJ, 447, 82
Schönrich R., Binney J., Dehnen W., 2010, MNRAS, 403, 1829
Sellwood J., Zanmar Sanchez R., 2010, MNRAS, 404, 1733
Siebert A. et al., 2008, MNRAS, 391, 793
Steinmetz M. et al., 2006, AJ, 132, 1645
Xu Y., Reid M. J., Zheng X. W., Menten K. M., 2006, Sci, 311, 54
Zwitter T. et al., 2008, AJ, 136, 421
Zwitter T. et al., 2010, A&A, submitted

This paper has been typeset from a TEX/LATEX file prepared by the author.